Review in Advance first posted online on April 13, 2009. (Minor changes may still occur before final publication online and in print.)

# Patient-Specific Modeling of Cardiovascular Mechanics

C.A. Taylor and C.A. Figueroa

Department of Bioengineering, Stanford University, Stanford, California; email: taylorca@stanford.edu, cafa@stanford.edu



Annu. Rev. Biomed. Eng. 2009. 11:109–34

The *Annual Review of Biomedical Engineering* is online at bioeng.annualreviews.org

This article's doi: 10.1146/annurev.bioeng.10.061807.160521



1523-9829/09/0815-0109$20.00

## Key Words

hemodynamics, imaging, atherosclerosis, aneurysms, congenital heart disease

## Abstract

Advances in numerical methods and three-dimensional imaging techniques have enabled the quantification of cardiovascular mechanics in subject-specific anatomic and physiologic models. Patient-specific models are being used to guide cell culture and animal experiments and test hypotheses related to the role of biomechanical factors in vascular diseases. Furthermore, biomechanical models based on noninvasive medical imaging could provide invaluable data on the in vivo service environment where cardiovascular devices are employed and on the effect of the devices on physiologic function. Finally, the patient-specific modeling has enabled an entirely new application of cardiovascular mechanics, namely predicting outcomes of alternate therapeutic interventions for individual patients. We review methods to create anatomic and physiologic models, obtain properties, assign boundary conditions, and solve the equations governing blood flow and vessel wall dynamics. Applications of patient-specific models of cardiovascular mechanics are presented, followed by a discussion of the challenges and opportunities that lie ahead.

## Contents

INTRODUCTION ..... 110
METHODS OF PATIENT-SPECIFIC MODELING
OF CARDIOVASCULAR MECHANICS ..... 111
Acquisition of Patient-Specific Anatomic and Physiologic Data ..... 111
Image Segmentation and Image-Based Geometric Modeling ..... 112
Automatic Mesh Generation ..... 114
Patient-Specific Physiologic Models and Boundary Conditions ..... 114
Numerical Methods for Fluid-Structure Interactions ..... 117
APPLICATIONS ..... 119
Disease Research ..... 119
Predictive Medicine ..... 122
FUTURE CHALLENGES ..... 123
Patient-Specific Tissue Properties for Fluid-Structure Interactions ..... 123
Predicting Long-Term Outcomes Using Fluid-Solid Growth ..... 124
Optimal Treatment Plans ..... 126
Device Design and Evaluation ..... 126
Verification and Validation ..... 127

## INTRODUCTION

At every stage of the circulatory system, whether blood is swirling in the heart or streaming through the arterial tree, a range of mathematical models have been employed to quantify biomechanical conditions. These models, ranging from lumped parameter, one-dimensional (1D) wave propagation, and three-dimensional (3D) numerical methods, can all be used with effect to describe cardiovascular mechanics. Computational methods were first applied to compute velocity and pressure fields in idealized, generic models of vascular anatomy and physiology. With the development of modern 3D imaging techniques, especially magnetic resonance and computed tomography imaging, it is now possible to quantify cardiovascular mechanics in subject-specific anatomic and physiologic models.

Development of image-based modeling technologies for simulating blood flow began in the late 1990s (1–3). Since that time, many groups have developed and utilized these techniques to investigate the pathogenesis of occlusive and aneurysmal disease in the carotid artery (4, 5), the coronary arteries (6), the aorta (7), and the cerebral circulation (8–10). Patient-specific modeling techniques have also been applied in solid mechanics analyses to predict rupture risk of aneurysms (11).

Furthermore, patient-specific models of cardiovascular mechanics can play an important role in the development of medical devices. The design and evaluation of medical devices necessitates gathering information on the following: the clinical problem that needs to be solved and the intended function of the device, the dynamic 3D anatomy of the portion of the body where the device will be deployed and the anatomic variability between subjects, the forces the body exerts on the device under a range of physiologic conditions, the mechanical performance of the device when subject to repetitive in vivo forces, and the biological and mechanical impact of the device on the body. Biomechanical models based on noninvasive medical imaging could provide invaluable data on the in vivo service environment where devices are employed and on the effect of the devices

on physiologic function. At present, medical device manufacturers have little information on the anatomic variations, the arterial deformation, and the biomechanical forces in the vascular system that are needed for the design of stents for occlusive disease and stent grafts to isolate aneurysms.

Finally, the construction of subject-specific geometric models from medical imaging data has enabled an entirely new application of cardiovascular mechanics, namely the prediction of changes in blood flow resulting from possible therapeutic interventions for individual patients. Patient-specific modeling of cardiovascular mechanics requires methods to (*a*) construct geometric models from 3D magnetic resonance imaging (MRI), computed tomography (CT), and ultrasound (US) data; (*b*) extract preoperative physiologic data from cine phase contrast MRI, US, or cardiac catheterization data; (*c*) modify the preoperative model to incorporate an operative plan; (*d*) assign boundary conditions incorporating upstream heart models and downstream microcirculation models; (*e*) discretize geometric models using automatic mesh generators; (*f*) solve the equations governing blood flow and vessel-wall dynamics; and (*g*) visualize and quantify resulting physiologic information. Recent progress in developing patient-specific models of cardiovascular mechanics for treatment planning are presented in this review, followed by a discussion of the challenges and opportunities that lie ahead. In closing, sensitivity analysis, verification, and experimental validation of patient-specific models of cardiovascular mechanics are described.

## METHODS OF PATIENT-SPECIFIC MODELING OF CARDIOVASCULAR MECHANICS

### Acquisition of Patient-Specific Anatomic and Physiologic Data

Methods for quantifying vascular anatomy for patient-specific modeling of cardiovascular mechanics include noninvasive imaging techniques such as CT, MRI, 3D ultrasound (3DUS), and an invasive method combining angiography and intravascular ultrasound (IVUS). Contrast-enhanced CT and MRI are particularly suited for generating high-resolution volumetric images of many parts of the vascular tree and are briefly described below. Generally, iodinated contrast is used in CT angiography, and a gadolinium-based contrast agent is used in magnetic resonance (MR) angiography. MRI has the additional advantage of being able to quantify physiologic parameters, including blood flow, wall motion, and blood oxygenation.

MRI is based on spatial localization of signals emitted by material (generally hydrogen nuclei for living organisms) exposed to radiofrequency (RF) magnetic field gradients (12). MR images are formed by applying magnetic field gradients in orthogonal directions to spatially encode the MR signal. A large number of pulse sequence repetitions are executed, each collecting a portion of the needed data. In two-dimensional (2D) imaging, spins in a thin (e.g., 2–10 mm) slice are excited using selective excitation. In direct 3D acquisitions, thinner contiguous slices can be imaged, and a better signal-to-noise ratio (SNR) can be obtained than with multiple 2D acquisitions, at the possible cost of a longer scan time. Contrast-enhanced MR angiography (CE-MRA) generally utilizes direct 3D acquisitions, allowing for thin slices (∼2–3 mm) to be acquired with a sufficient signal-to-noise ratio. CE-MRA, based on fast gradient echo sequences, can be used to acquire a time-averaged volume of data in a single breath-hold. The use of MR data in patient-specific modeling requires correction for gradient nonlinearities arising during acquisition to avoid image distortion in the slice direction of the magnetic field, the so-called grad warping phenomena (13).

CT images are created by acquiring projection X-ray images as the gantry rotates around an object and then reconstructing cross sections depicting the density variation (attenuation coefficient) in the object. Modern clinical CT allows visualization of detail as small as 0.5 mm in-plane, with a slice thickness that is typically 0.75 mm. Temporal resolution, the time required for the

acquisition of projection data used to reconstruct an image, is most important for dynamic applications, especially coronary CT angiography. Independent of the reconstruction technique, the temporal resolution is proportional to the gantry rotation period, typically less than 0.5 sec for recent commercial scanners. In cardiac gated imaging, if the cardiac or vascular motion can be assumed to be fairly periodic, data from multiple rotations can be combined to achieve temporal resolution that is well shorter than the rotation period. Advanced reconstruction algorithms can achieve temporal resolutions of less than 100 ms (14), and up to 10 phases can be reconstructed through the cardiac cycle. Note that this technique relies upon quasi-periodicity of the motion.

Systemic and pulmonary blood flow has been measured extensively in vivo using invasive methods. These techniques employ fluorescent microspheres, electromagnetic flowmeters, laser Doppler anemometry, scintigraphy, and catheterization. Unfortunately, fluorescent microspheres, electromagnetic flowmeters, and laser Doppler anemometry are highly invasive and, as a result, are not currently used for blood-flow measurement in patients. Currently, the gold standard for cardiac output quantification uses invasive cardiac catheterization. Although these methods enable quantification of average cardiac output, they cannot measure the 3D, pulsatile characteristics of blood flow that are needed in patient-specific models of cardiovascular mechanics relevant to congenital and acquired cardiovascular diseases.

The current techniques to measure blood flow noninvasively include Doppler ultrasound and MRI. Doppler ultrasonography can acquire time-resolved blood velocities; however, it cannot resolve a velocity map on an arbitrarily oriented anatomic plane. Phase contrast MRI (PC-MRI) can noninvasively and concurrently acquire anatomic data and 3D velocity maps of blood flow in large vessels (15–17). The data acquired at each pixel in an MR image represents the transverse magnetization and is a vector quantity (i.e., it has a magnitude and phase). Typically, only the magnitude information is used to create an MR image, and the phase information is discarded; however, the phase can be used to quantitatively image motion (15–17). To encode flow in the x, y, or z direction, a bipolar gradient pulse can be added to the gradient waveform in that particular direction. To image velocity in a single direction, two-phase images are obtained with different values of the gradient first moment in the desired direction. These images are subtracted to remove irrelevant phase effects to produce an image that is proportional to the change in first moment and the velocity. Sensitivity to velocity can be adjusted and is parameterized by the velocity encoding that produces a phase shift of 180°. Three component vector velocities can be measured by making four other measurements (15): one reference and three where the first moment along x, y, or z are switched. For the high-spatial-resolution images needed for many applications, all the raw data needed to form the desired images cannot be obtained in a single cardiac cycle. Instead, a large number of pulse sequence repetitions are executed, each collecting a portion of all the needed data. Assuming periodicity, some form of gating or synchronization of these repetitions enables the resolution of motion as a function of time in the cardiac cycle. In the cine method, data are collected continuously throughout the cycle, and the data are retrospectively sorted and interpolated to produce a number of frames as a function of time in the cycle. Cine imaging can be combined with PC-MRI to generate velocity images as a function of time in the cardiac cycle.

## Image Segmentation and Image-Based Geometric Modeling

Image segmentation can be defined as the division of an image into meaningful regions. Low-level segmentation techniques (e.g., thresholding and region-growing methods) depend on per-pixel information such as image intensity, whereas high-level techniques, such as split-and-merge, pattern-recognition and texture-based methods, depend on the spatial distribution of data (e.g., image features) (18). Geometric segmentation techniques, sometimes referred to as active contours

or deformable models, synthesize both low-level and high-level image information and maintain the spatial relationships among image features (19). Geometric image segmentation techniques use deforming contours (curves and surfaces) to detect structures in images. Energy terms (typically one term indicative of the smoothness of the contour and another indicative of how near it lies to gradients in the image) are used to deform the contour while minimizing its energy (19, 20). This approach suffers from two primary drawbacks (21). First, the final segmentation result can be a strong function of initialization. Second, if explicit boundary-tracking methods are used to describe a deforming contour, arbitrary changes in contour topology cannot be handled. Among the refinements developed to address the first drawback was the balloon force introduced in Reference 22, which gives an inflationary behavior to the deforming contour. This can enable the contour to move past local minima, making it less sensitive to initialization. To address the issue of topological change, Malladi et al. (23) and Caselles et al. (24) successfully applied the level set method to the active contour approach. The level set method (see Reference 25) is an implicit boundary-tracking technique that eliminates many of the difficulties encountered when modeling evolving curves and surfaces with more traditional techniques. It embeds geometry into a scalar field such that the geometry's evolution can be described with a partial differential equation. A particular strength of the level set method is that it handles arbitrary topological changes and that it can be extended with relative ease to higher dimensions. Several researchers have described the application of level set methods to 3D segmentation problems (23, 26, 27).

Typically, geometric solid-models of blood vessels have been constructed by (*a*) extracting a set of points (a contour) approximating the inside boundary of a vessel on a series of 2D image slices, (*b*) interpolating the contour with a curve, (*c*) lofting a surface through the interpolated curves, and (*d*) joining the surfaces together to form a bounded volume. Wang et al. describes methods for constructing subject-specific vascular models based on volumetric MRA and CT images (28). This approach includes image segmentation techniques based on the level set method for vascular profile extraction and model construction using surface lofting with axis-normal profiles. **Figure 1** depicts a geometric model of an abdominal aorta created using this approach (7).

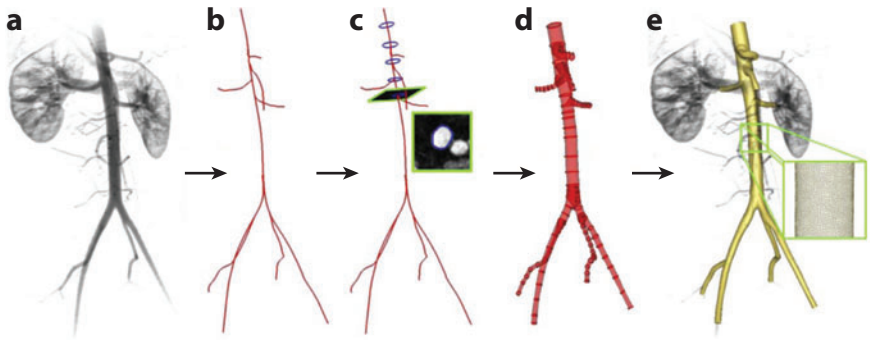


**Figure 1**

Schematic of solid-model construction from imaging data. (*a*) Volume-rendered image of a contrast-enhanced magnetic resonance angiogram illustrating abdominal aortic anatomy. (*b*) Centerline paths were created along the vessels of interest. (*c*) Two-dimensional (2D) segmentations of vessel lumen were taken perpendicular to the vessel path. Segmentations were found using a level-set method. (*d*) 2D segmentations were lofted to form solid models for each vessel, which were then joined to form a complete three-dimensional (3D) solid model of the aorta and its branches. (*e*) The solid model was discretized into a finite-element mesh (*gold*) and is shown with the original volume-rendered magnetic resonance angiogram (7, 104).

A particular advantage of the 2D segmentation and surface lofting approach is that complex geometries can be created even when there are regions of the volumetric image data with lower signal-to-noise ratio, as occurs in many, if not most, practical examples. As a result, very complex geometric models with numerous branch vessels can be created. However, this enhanced user control comes at the expense of user time. Specifically, a user must often manually identify the set of imaging slices needed to represent a feature, initialize and fine-tune the segmentation, and evaluate and refine the curve and surface interpolations. This is especially time-consuming at complicated anatomic regions such as vessel branches. The accuracy of current geometric models constructed using these methods can also be an issue because a 3D model is constructed using only local 2D information from the inherently 3D volumetric data.

In the past several years, there has been an increased tendency to utilize 3D segmentation methods, extract triangulated surface meshes, and then generate volumetric meshes (29–32). Bekkers & Taylor recently described an alternative method for the generation of image-based, 3D, multi-scale vascular models (33). The method generates multi-scale surfaces based on either a linear triangulation or a globally smooth nonuniform rational b-spline (NURB) representation using subdivision surface techniques. A novel hierarchical global topology and feature analysis drives surface generation. The method is particularly suited for blood-flow modeling of very large vascular models with a wide range in vessel sizes where adaptive mesh refinement based on flow features makes an underlying smooth surface representation desirable.

## Automatic Mesh Generation

As noted by Prakash & Ethier (34), mesh refinement studies are rarely reported in the computational hemodynamics literature. Indeed, as mesh independence of solutions is not reported, it is likely that many of the reported solutions are under resolved. Notably, complex recirculating flow features observed in many experimental fluid mechanics studies of blood flow are typically not seen in computational simulations (35, 36). Adaptive mesh generation techniques were recently described for computational hemodynamics studies. Muller et al. (37) and Sahni et al. (38) discuss a method whereby a posteriori error estimators, based on the Hessian of the velocity magnitude (speed) field, provide necessary information to adaptively refine a finite-element mesh. Directional information on the solution error can be used to generate anisotropic elements with greater refinement in the directions of steepest changes in velocity gradients (e.g., the radial direction). Furthermore, because resolution of wall shear stress is often of interest, boundary-layer mesh generation techniques can be used to increase mesh density near the vessel wall (39). **Figure 2** depicts an anisotropic, adapted boundary-layer mesh for a healthy human abdominal aorta. Such mesh generation techniques will be necessary for obtaining mesh-independent solutions for patient-specific models of blood flow.

## Patient-Specific Physiologic Models and Boundary Conditions

Early 3D simulations of blood flow in arteries focused on the velocity field and derived quantities such as wall shear stress (1, 40, 41). Velocity profiles were prescribed at the inlet and outlets to achieve a desired flow distribution, and a constant, generally zero, normal traction was prescribed at one or more outlets. As a result, blood pressure levels were not computed accurately, and simulations could not be performed where the flow distribution and pressure field were part of the desired solution. For example, this approach precluded models of wave propagation, resulted in unrealistic fluid-structure interaction simulations, and negated the possibility of predicting outcomes of interventions. Athough one might be tempted to prescribe pressure waveforms at

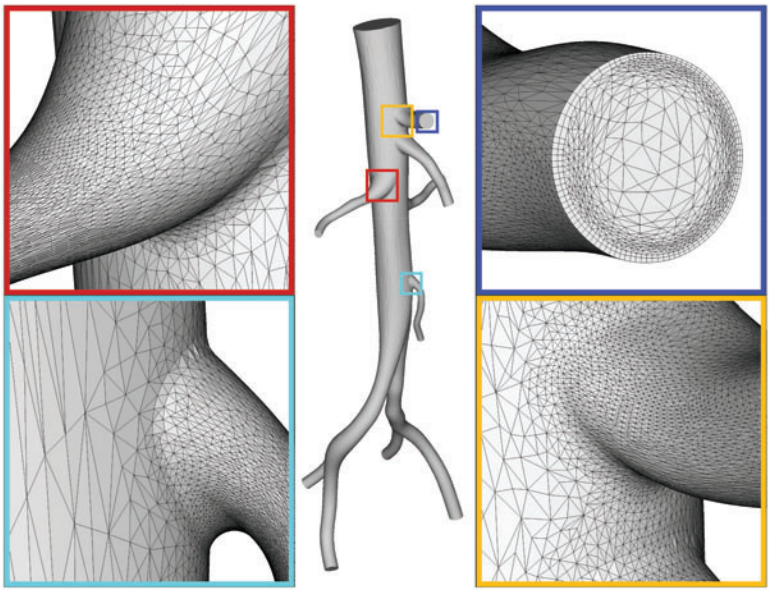

**Figure 2**

Anisotropic, adapted, boundary layer mesh for a healthy human abdominal aorta. A boundary layer mesh is observed in the top right panel, and anisotropic elements are highlighted in the bottom left panel (figure courtesy of Dr. Kenneth Jansen).

the inlet or outlets, this approach fails for multi-branched models or deformable models because pressure and flow wave amplitude, shape, and phase depend on the solution in the modeled domain and cannot be assigned a priori. The inability to model pressure-wave propagation has led to a singular focus on wall shear stress as the primary hemodynamic factor contributing to atherogenesis, aneurysm initiation, and enlargement.

An alternative to prescribing velocity profiles or pressure at inlet or outlet boundaries is to couple flow rate and pressure in the numerical domain to a reduced-order model, i.e., a 1D network or zero-dimensional (lumped) model (2, 42–45). This approach can be applied at the inlet or outlet boundaries of the patient-specific numerical model. The combined patient-specific and reduced-order-model problem can be solved in an explicit, staggered manner or, preferably, by embedding the reduced-order model into the variational equations of the patient-specific model, as is done in the coupled multidomain method (44, 46). This latter, implicit-coupling approach results in a stable, efficient formulation that, together with 1D linear wave propagation theory, can be used to couple distributed models with tens of millions of branches to numerical models (47). For the 1D network models, branching patterns, length, diameter, and material properties of vessel segments are assigned; whereas for the lumped-parameter models, resistance, capacitance, inductance parameters, and elastance functions (for lumped heart models) are set to achieve the desired hemodynamic characteristics of the upstream or downstream domain. Numerical optimization methods can be employed to tune the parameter values of the reduced-order models to match measured flow distribution or pressure values in the patient-specific model (48). Using this approach to boundary condition specification, flow distribution and pressure wave propagation arise naturally through the coupling between the patient-specific 3D model and the reduced-order model (44, 49). **Figure 3** depicts an application of this approach to modeling blood flow in the pulmonary arteries of a 16-year-old male with repaired tetralogy of Fallot and left

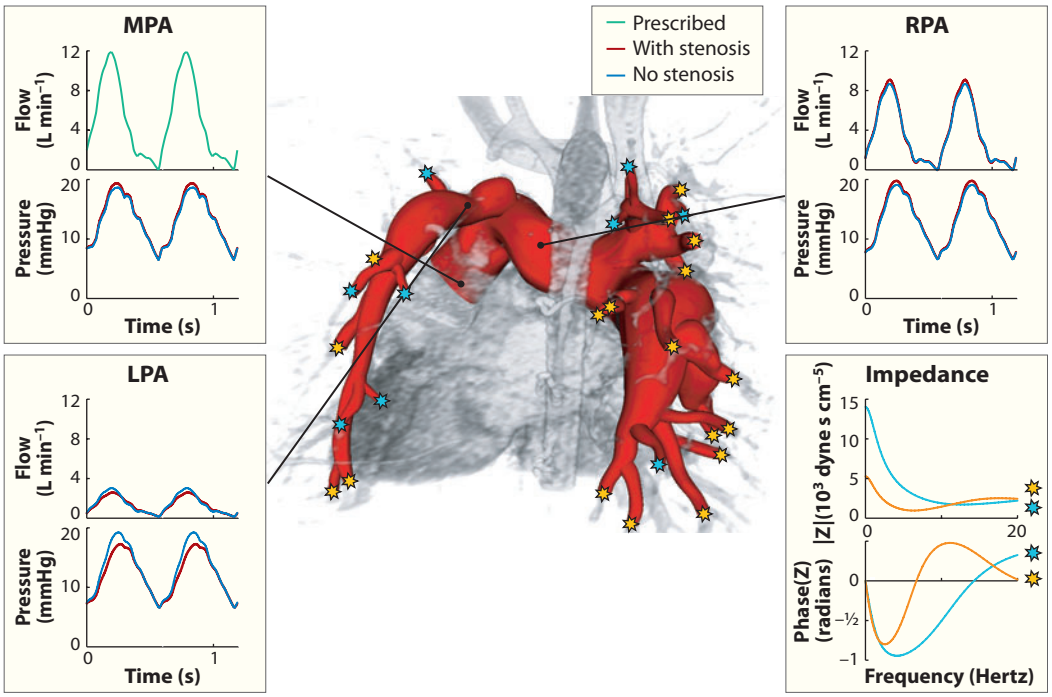


**Figure 3**

Simulation of blood flow in the pulmonary arteries of a 16-year-old male with repaired tetralogy of Fallot and left pulmonary arterial stenosis. Main, right, and left pulmonary arterial flow and pressure are shown for simulations performed with and without left pulmonary artery stenosis. Main pulmonary arterial flow and morphometry-based impedance outlet boundary conditions were prescribed. The predicted blood flow to the left lung is less than that to the right lung and is unaffected by removal of the stenosis (47).

pulmonary arterial stenosis. Main, right, and left pulmonary arterial flow and pressure are shown for simulations performed with and without left pulmonary artery stenosis. Main pulmonary arterial flow was prescribed at the inlet of the computational model, and morphometry-based impedance boundary conditions were prescribed at each outlet (28). Although, in this case, a 1D nonlinear wave-propagation model was used in the upstream domain, this example illustrates the importance of assigning realistic boundary conditions in patient-specific blood flow simulations.

A relatively new development in boundary-condition specification has arisen as a result of difficulties in solving a class of problems in which the patient-specific model is truncated in a region where flow is complex, recirculating, or retrograde, and a weakly enforced lumped-parameter or distributed reduced-order model is used to represent the downstream domain. Such numerical difficulties are inherent in problems related to modeling hemodynamics in the aorta or pulmonary arteries. Formaggia et al. (50) described a method, the total-pressure boundary condition, to control the energy flux entering and exiting the computational domain and to stabilize problems with complex flows near boundaries. However, this approach requires an unconventional formulation of the Navier-Stokes equations and has not yet been proven to resolve boundary instability issues in complex hemodynamic simulations. An alternate solution to this problem, proposed by Kim et al. (51), is to use the augmented Lagrangian method to constrain the shape (but not the magnitude) of the velocity profile at inlet or outlet boundaries. This approach, applied to the same boundaries where a lumped-parameter or distributed-network boundary condition is

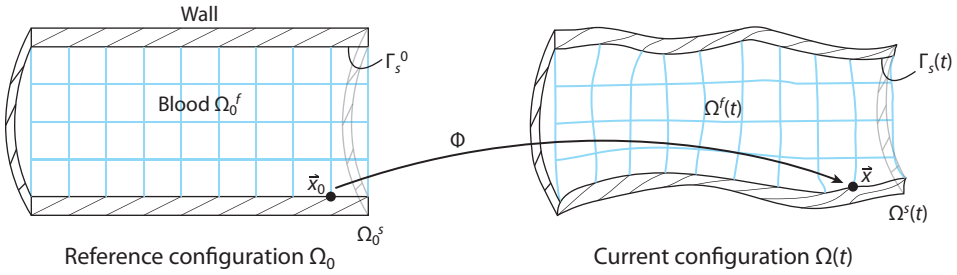


**Figure 4**

Configurations of the blood and vascular structure domains.

assigned, has the remarkable effect of stabilizing many problems with complex flows near outlet boundaries.

## Numerical Methods for Fluid-Structure Interactions

Blood can be accurately represented as an incompressible fluid, the constitutive behavior of which is usually approximated by a Newtonian model. Arterial blood flow has been traditionally represented using the incompressible Navier-Stokes equations in a fixed Eulerian frame of reference. However, blood velocity and pressure fields can be greatly influenced by the motion of external or internal vascular structures, such as the contracting cardiac muscle, moving heart valves, or deforming large arteries of the body. In these situations, one must characterize the mechanical behavior of the moving vascular structure (usually in a Lagrangian frame of reference) and its interactions with the blood flow. Modeling the interactions between an incompressible blood flow and a deforming vascular structure represents one of the major challenges in the field of cardiovascular mechanics.

**Arbitrary Lagrangian-Eulerian formulations.** One of the most well known techniques used to describe fluid-structure interaction (FSI) is the arbitrary Lagrangian-Eulerian (ALE) formulation (52, 53). In this formulation, the Navier-Stokes equations are written in a moving reference frame that follows the motion of the vascular structure interface $\Gamma_s(t)$ (see **Figure 4**). The evolution of this interface is determined by kinematic (continuity of velocities) and dynamic (continuity of forces) compatibility conditions between the blood flow and the vascular structure. In ALE formulations, the motion of the blood-flow computational grid is arbitrary and defined by a grid velocity $\vec{v}_G \equiv (\partial\vec{x}/\partial t)|_{\vec{x}_0}$. This velocity is defined by the Lagrangian motion of the vascular structure at the fluid-solid interface $\Gamma_s(t)$, but it needs to be generalized for the grid points of the flow domain not in contact with the vascular structure.

In an ALE formulation, one must therefore solve the following three-field problem:

1. The Navier-Stokes equations of motion of a fluid in a moving domain $\Omega^f(t)$, to represent the blood motion,

$$\begin{aligned} &\nabla_{\vec{x}} \cdot \vec{v} = 0 \\ &\rho \left.\frac{\partial \vec{v}}{\partial t}\right|_{\vec{x}_0} + \nabla_{\vec{x}} \cdot (\rho \vec{v} \otimes (\vec{v} - \vec{v}_G)) = \nabla_{\vec{x}} \cdot (\underset{\sim}{\sigma}) + \vec{f} \end{aligned} \qquad \text{in} \Omega^f(t). \tag{1}$$

2. The elastodynamics equations of motion of the vascular structure $\Omega^s(t)$, usually written in a Lagrangian frame of reference with respect to some initial configuration $\Omega_0^s$,

$$\rho_0 \frac{\partial \vec{v}}{\partial t} + \nabla_0 \cdot (\underset{\sim}{\sigma}\, F^{-T}) = \vec{f}_0 \qquad \text{in } \Omega_0^s. \tag{2}$$

3. The motion of the computational grid for the blood flow over an interval $I$, defined by an arbitrary mapping $\Phi$ that matches the structure motion at the interface $\Gamma_s(t)$,

$$\begin{aligned} &\Phi : \Omega_0 \times I \rightarrow \Omega(t) \\ &(\vec{x}_0, t) \rightarrow \vec{x} = \Phi(\vec{x}_0, t). \\ &\Phi(\vec{x}_0, t) \in \Gamma_s(t) \quad \forall \vec{x}_0 \in \Gamma_0^s \end{aligned} \tag{3}$$

The evolution of the ALE formulation is a boundary-fitting technique, where the fluid-solid interface is accurately captured due to continuous changes of the fluid grid. However, in situations in which the motion of the vascular structure is large, ALE formulations may result in time-consuming computations. Currently, modular (also known as staggered) and nonmodular (also known as monolithic) preconditioners for the solution of the coupled algebraic system resulting from the space-time discretization of the FSI problem represent an active area of research. Modular preconditioners allow for the use of independent, specialized fluid and structure solvers coupled via a relatively simple iterative scheme. However, these algorithms usually exhibit poor convergence behavior, especially in problems with large added mass effect, where the density of the structure is comparable to the density of the fluid, as occurs in cardiovascular FSI problems. Alternatively, nonmodular preconditioners require a more elaborate coupling between the fluid and solid solvers, but they usually result in faster, more stable algorithms. Geometric conservation laws that govern the evolution of geometric parameters, including grid positions and velocities, have been developed to avoid overly diffusive grid-motion strategies. A geometric conservation law requires that motion of grid is computed in a way such that the numerical scheme is able to reproduce exactly a constant solution. The use of ALE formulations in cardiovascular applications was pioneered by Perktold and collaborators (54, 55). More recently, Gerbeau and colleagues (56–58) performed pressure wave propagation simulations in cerebral-aneurysm and carotid-bifurcation models, Hughes and colleagues (59, 60) performed patient-specific FSI simulations using an isogeometric framework, and Van de Vosse and colleagues (61) investigated a patient-specific abdominal aortic aneurysm model.

**Immersed-boundary-method formulations.** The immersed boundary method, first introduced by Peskin (62, 63), is a nonboundary-fitting formulation that does not require any changes on the fluid computational grid. This formulation was first developed in the context of finite-difference approximations for the fluid domain, with a set of nonconforming, interconnected, elastic boundary points representing the structure. This structure interacts with the fluid via the introduction of body forces applied on the fluid domain at the position of the solid points. The immersed boundary method has been used in cardiovascular applications by Lemmon & Yoganathan (64) to examine left ventricular dysfunction, by Watton et al. (65) to study prosthetic mitral valves, and by Vigmond et al. (66) to develop a whole-heart electro-mechano-fluidic computational framework. On the microscales, the immersed boundary method has also been applied to modeling the interactions of red blood cells and plasma in the mesocirculation (67).

**Fictitious domain formulations.** The fictitious domain method was first developed by Glowinski et al. (68). Although closely related to the immersed boundary method, the fictitious domain method was developed in a finite-element context, introducing Lagrange multipliers to constrain the motion of the fluid and the solid at the interface. Later, Baaijens (69) developed an extension of the method that is suitable for slender structures. The method has been successfully applied to FSI simulations of the aortic valve (70, 71). Van de Vosse and colleagues (72) proposed a combination of ALE and fictitious domain methods, and they applied it to the simulation of valve dynamics

in simple left-ventricular-flow models. More recently, Van Loon et al. (73) used a similar hybrid approach to solve a heart-valve-dynamics problem.

**Deforming spatial domain/stabilized space-time method.** In this formulation developed by Tezduyar et al. (74), the deforming spatial domain is handled by using space-time finite-element spaces. Here, the motion of the unknown boundary is defined in terms of other variables, such as velocities or displacements of the interface. This formulation has been applied to study FSI in a patient-specific model of a cerebral aneursym (32).

**Coupled-momentum method.** Figueroa, Taylor, and colleagues (49) recently developed a coupled-momentum method to simulate blood flow and vessel deformation in arteries. This method embeds the elastodynamics equations into the variational form of the fluid via the definition of a fictitious body force that drives the motion of the vessel. By using a thin-wall assumption, this body force is related to the traction at the fluid-solid interface. The formulation results in a robust, monolithic scheme that is highly efficient for large-scale fluid-structure interaction and wave-propagation problems, provided that the assumptions of small deformation and thin walls are reasonable. For example, **Figure 5** shows results from a patient-specific model of blood flow from the aorta to the cerebral arteries for a patient with a right-middle cerebral aneurysm. This computation included 3-element Windkessel outlet boundary conditions implemented using the coupled multidomain method (44), constraints on the shape of outlet velocity profiles (51), and fluid-structure interactions, including spatially varying tissue properties modeled using the coupled momentum method (49). **Figure 6** depicts the velocity magnitude and pressure fields at peak systole and at mid-diastole for a patient-specific simulation of blood flow and vessel dynamics in the aorta of a 10-year-old patient with aortic coarctation (75). In this simulation, the coupled multidomain method (44) and augmented Lagrangian methods (51) are used to couple the 3D patient-specific model to a lumped-parameter heart model at the inlet and 3-element Windkessel models at the outlets and to constrain the shape of velocity profiles at inlet and outlet boundaries. The coupled momentum method (49) was used to solve the fluid-structure-interaction problem on a finite-element mesh with 2,647,619 elements, 475,866 nodes, and a time-step size of 0.025 ms.

**Future challenges in fluid-structure interactions.** New imaging techniques enable the characterization of the motion and thickness of vascular structures; however, it remains a challenge to incorporate this in vivo information into FSI formulations. A new class of image-based FSI problems will require the development of methods to assign tissue properties to the computer model from the medical image data, via the solution of an inverse problem.

## APPLICATIONS

### Disease Research

The role of hemodynamic conditions in the pathogenesis of cardiovascular diseases is now widely accepted in large part because of seminal research correlating experimental fluid mechanical measurements with observed pathology. Early research using computational methods to quantify hemodynamic conditions followed the lead of the prior experimental studies by using idealized anatomic models and boundary conditions. The advent of methods for patient-specific modeling of cardiovascular mechanics has enabled researchers interested in the role of hemodynamics in cardiovascular disease to construct anatomic and physiologic models of individuals, perform subject-specific simulations, and extract subject-specific hemodynamic conditions. Such methods

**Figure 5**

Volume rendering of velocity magnitude for patient-specific model of blood flow from aorta to cerebral arteries for a patient with a right-middle cerebral aneurysm. Simulation results are visualized together with computed tomography (CT) image data to provide anatomic context.

offer a significant advantage over the use of idealized models in that they can be used to identify common hemodynamic features across a range of subjects, examine inter-subject variability, and draw statistically meaningful conclusions about hemodynamic variables. The majority of applications of patient-specific modeling of cardiovascular mechanics have focused on hemodynamic factors in atherosclerotic and aneurysmal disease.

**Atherosclerosis.** Atherosclerosis, the most prevalent of the acquired cardiovascular diseases, involves the accumulation of fatty material in the intima (inner layer) of arteries supplying the brain, heart, other vital organs, and lower extremities. However, although the biochemical stimuli for the development of atherosclerosis are diffuse throughout the body, the disease is very focal, localizing at branches and bends of the arterial tree. There is substantial and mounting evidence for the role of hemodynamic factors in the localization of atherosclerosis (76–78). Atherosclerotic arteries continue to adapt in response to hemodynamic forces, by a mechanism known as

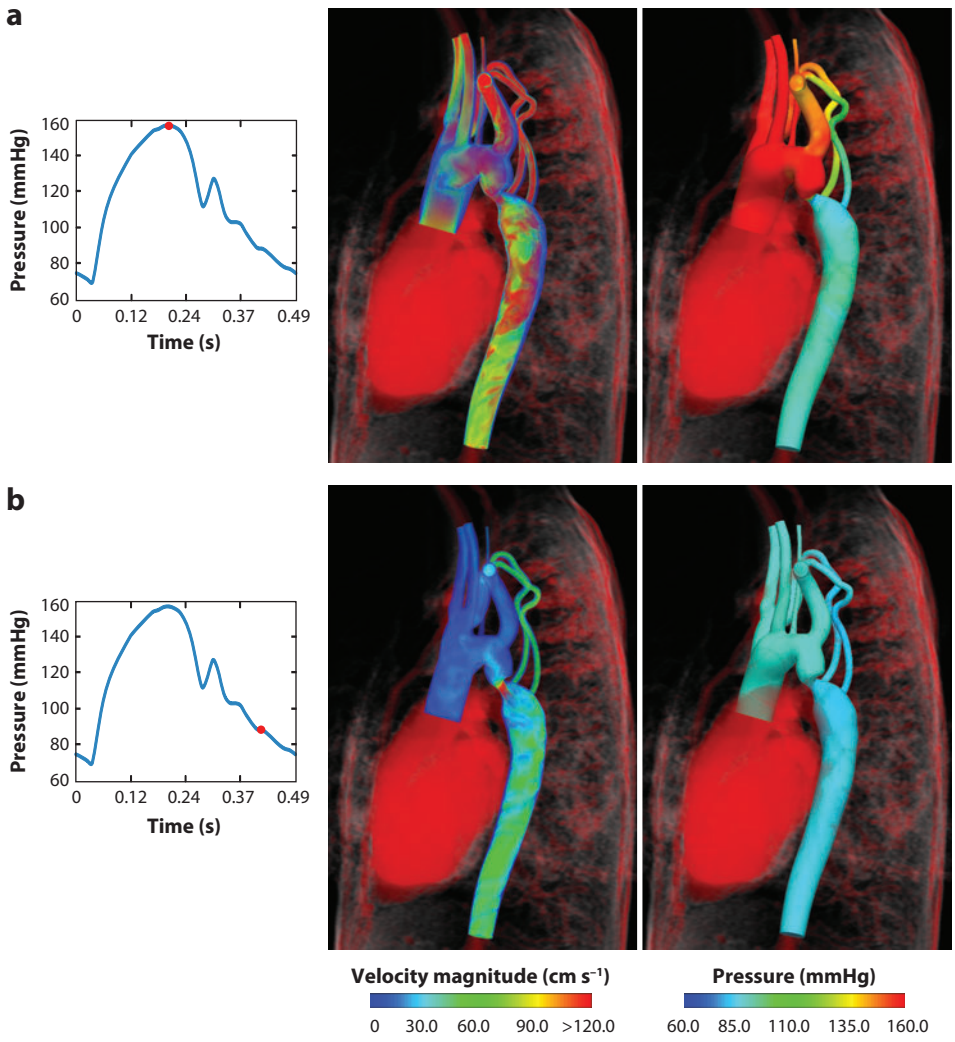


**Figure 6**

Velocity magnitude and pressure fields at (*a*) peak systole and (*b*) mid-diastole for a patient-specific simulation of blood flow and vessel dynamics in the aorta of a 10-year-old patient with aortic coarctation.

compensatory remodeling (79). Patient-specific models have been widely used to quantify hemodynamic conditions in arteries for the purpose of understanding localization of atherosclerosis.

Owing to the strong correlation between hemodynamics and atherosclerosis in the carotid bifurcation, it is not surprising that this vascular region has been widely studied. In particular, the Steinman group at the University of Western Ontario and the Ethier group at the University of Toronto have made important contributions to the field (5, 80–83). The Xu group at Imperial College in London have also made significant contributions toward understanding hemodynamic conditions in the carotid artery (84, 85). Recently, Gimbrone's lab at Harvard described phenotypic differences in endothelial cells exposed to different shear stress waveforms characterized using image-based modeling techniques in the carotid artery bifurcation (86).

The infrarenal abdominal aorta is another site prone to atherosclerosis, likely due to unique hemodynamic conditions, including low wall shear stress, high oscillatory shear, and generally low flow, particularly for sedentary individuals (41, 87–91). Tang et al. reported the hemodynamic conditions under resting and exercise conditions in five patient-specific models of the abdominal aorta (7). When averaged over all subjects, wall shear stress significantly increased, whereas oscillatory shear index (OSI) decreased between rest and exercise at the supraceliac, infrarenal, and suprabifurcation levels, and significant differences in wall shear stress were found between anterior and posterior sections. Of note, in the atherosclerosis-prone infrarenal aorta, wall shear stress increased sixfold between rest and exercise.

Finally, with the advent of small-animal imaging, image-based modeling techniques have been applied to quantify hemodynamic conditions in rodent models often used for disease research. For example, using magnetic resonance imaging and computational methods, Greve et al. showed that shear stress varies across species in relation to body mass, according to the allometric law $\tau \sim M^{-3/8}$ (92). Importantly, wall shear stress in the aorta of a mouse is more than 20-fold higher than that in humans. Feintuch et al. (93) and Suo et al. (94) confirmed these findings using image-based modeling to examine hemodynamic conditions in the mouse aortic arch.

**Aneurysms.** The recent review by Humphrey & Taylor (95) thoroughly discusses the role of computational mechanics in intracranial saccular and abdominal aortic aneurysm research. As noted in their review, image-based modeling techniques have been used in the past few years to conduct patient-specific investigations with the aim of determining whether biomechanical factors influence aneurysm initiation, growth, and rupture (8–10, 96–101). In regard to hemodynamic forces, low wall shear stress, high wall shear stress, and elevated dynamic pressure have been proposed to influence aneurysm growth. For example, Acevedo-Bolton et al. (96) concluded that regions of basilar artery aneurysms that continued to enlarge experienced low wall shear stress. Very recently, using a longitudinal study of seven patients with inoperable cerebral aneurysms, Boussel et al. provided compelling data to support the hypothesis that regions of low wall shear stress exhibited the greatest propensity for aneurysm growth (102). Undoubtedly, patient-specific computational methods will be used increasingly by investigators studying aneurysm growth and rupture.

## Predictive Medicine

Interventional and surgical therapies used in the treatment of congenital and acquired cardiovascular diseases attempt to restore blood flow to compromised organs and tissues. Ideally, these therapies result in sufficient blood flow at appropriate physiologic pressures while avoiding adverse flow conditions, such as flow recirculation and stasis, that may lead to procedural failure and/or poor outcomes. Unfortunately, alternate treatments cannot be tested in the patients, and physicians do not have the tools needed to evaluate the multiple options and to design the optimal corrective procedures. Instead, the current paradigm for medical planning for the treatment of cardiovascular disease relies exclusively on diagnostic imaging data and physical measurements to define the present state of the patient, empirical data to evaluate the efficacy of prior treatments for similar patients, and the judgment and experience of the physician to decide on a preferred treatment. However, diagnostic imaging, physical measurements, and empirical data are insufficient to predict the outcome of a given treatment for an individual patient owing to anatomic and physiologic variations and system complexity.

In the new paradigm of predictive medicine, a physician utilizes computational tools to construct and evaluate a combined image-based anatomic/physiologic model to predict the outcome

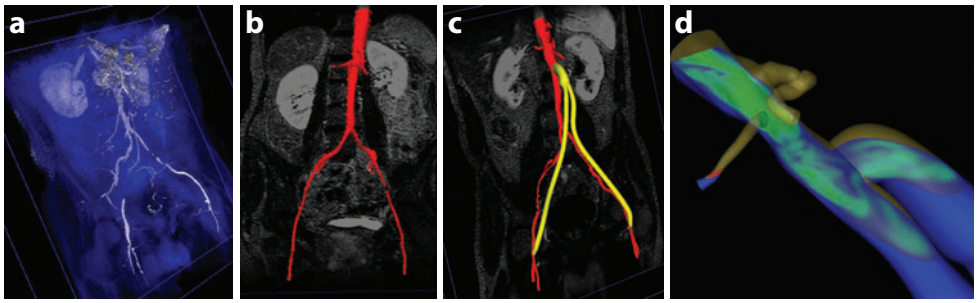


**Figure 7**

Overview of a simulation-based medical planning approach as applied to designing bypass surgery for patient with occlusive cardiovascular disease in the aorta and the iliac arteries. Shown from left are (*a*) magnetic resonance angiography data, (*b*) preoperative geometric solid model (*red*), (*c*) operative plan (proposed aortofemoral bypass graft shown in *yellow*), and (*d*) computed blood-flow velocity in the aorta and the proximal end of bypass (103).



of alternative treatment plans for an individual patient. For cardiovascular treatment planning, these simulation systems require an integrated set of software tools to model the effect of alternate treatments on blood flow. The key elements of such a system include a human-computer interface, image segmentation, geometric solid-modeling, operative planning, discretization methods, fluid-structure interaction methods, and scientific visualization techniques. Simulation-based medical planning systems must be efficient and minimize user intervention so that results can be obtained in minutes to hours instead of days to weeks. These systems must also accurately describe the key hemodynamic variables, especially flow rate and pressure.

In 1998, Taylor and colleagues developed a prototype software system, Advanced Surgical Planning Interactive Research Environment (ASPIRE), for patient-specific cardiovascular surgery planning using computational methods for modeling blood flow. ASPIRE was demonstrated in the plenary research forum at the 1998 Society for Vascular Surgery (SVS) meeting and was used successfully by four prominent vascular surgeons to evaluate alternate surgical plans for a case of lower extremity occlusive disease (2). Wilson et al. described the development of a new software system for image-based modeling and cardiovascular surgery planning, ASPIRE2 (103, 104). Modular software architecture was utilized to enable the use of best-in-class component technology and to create a single application to go from medical imaging data to analysis results. **Figure 7** provides an overview of the predictive medicine approach as applied to designing bypass surgery for a patient with occlusive cardiovascular disease in the aorta and the iliac arteries (103).

In the past several years, a few groups have started to apply image-based modeling techniques to the assessment of surgical procedures for patients with congenital heart diseases. Notable among these efforts is the work of Yoganathan and colleagues (105, 106) and Migliavacca, Bove, de Leval and colleagues (42, 43, 107–109) to assess the hemodynamic efficiency of the total cavopulmonary connection. Marsden et al. recently used image-based modeling techniques to design a novel surgical repair to replace the existing Fontan procedures (110).

## FUTURE CHALLENGES

### Patient-Specific Tissue Properties for Fluid-Structure Interactions

With the advent of more powerful image acquisition and processing techniques, the accuracy and complexity of patient-specific cardiovascular geometric models has increased dramatically.

However, the ever-improving level of sophistication of computational formulations for blood flow and vascular structure interactions requires more information than the mere definition of the vascular geometry: There is a pressing need to characterize the mechanical behavior of the vascular structure and the tissues around it. This behavior is represented not only by the stiffness, viscoelasticity, and mass of the tissues but also by the tethering conditions that structures such as bones and muscle impose on the vasculature. It is clear that given the large subject-to-subject variability of the cardiovascular system, the definition of the vascular and perivascular tissue properties must be made on a patient-specific basis. Best-fit values of the material parameters that characterize tissue behavior in vivo are challenging to define. New methods such as MRI-based elastography (111) and data assimilation techniques (112) need to be developed to assign tissue properties to cardiovascular geometric models.

## Predicting Long-Term Outcomes Using Fluid-Solid Growth

Blood vessels exhibit a remarkable ability to adapt throughout life: We observe normal vascular adaptations in development and aging; adaptations to injury, such as in wound healing and vasospasm; adaptations in disease, such as atherosclerosis and aneurysms; and adaptations to changes in the overall hemodynamic state of the subject, such as a chronic increase in flow in endurance training or a change in blood pressure, as in hypertension or microgravity. These adaptations represent changes in both the shape and material properties of the vessel and depend on an array of factors, such as gene pathways, complex biochemical processes in the vessel wall, and as many findings over the past few decades indicate, the mechanical environment of the vessel. Many observations at the subcellular, cellular, and even cell-matrix levels point to the existence of a preferred or homeostatic mechanical state across multiple spatial and temporal scales. Thus, it is thought that vascular growth and remodeling (G&R) happens in response to a significant alteration of the homeostatic state of a vessel (113).

Changes in the shape and mechanical properties of blood vessels are ultimately related to changes in its constituents: resident cells (smooth muscle and endothelial cells) and the extracellular matrix. The main remodeling agents in the vessel wall are the endothelial cells, vascular smooth muscle cells, and fibroblasts. Many studies have attempted to elucidate the role of each of these elements in arterial G&R. From a computational standpoint, two main methodologies have been proposed: the kinematic-growth approach (114, 115) and the constrained-mixture approach (116–118). The kinematic-growth approach models the G&R without representing the underlying bio-chemo-mechanical mechanisms modulating growth. The constrained mixture framework incorporates the response of smooth muscle and collagen fibers to changes in mechanical loading, based on mass-density production and removal functions. These responses can be characterized via the combination of adequate cell-culture experiments and computational methods to model hemodynamic-induced loads on the vascular wall (113), such as cyclic stretch (or stress) and wall shear stress. For example, smooth muscle cells can increase their production of collagen in response to changes in intramural loading. Conversely, these cells can increase the production of matrix metalloproteinases (MMPs), responsible for selective degradation of collagen and elastin, in response to the same mechanical stimulus (119). Furthermore, the endothelial layer can increase the production of nitric oxide (NO), a potent vasodilator, in response to local increases in wall shear stress levels. Conversely, endothelial cells can increase the production of endothelin-1 (ET-1), a potent vasoconstrictor, in response to decreases in wall shear stress. However, NO is also an inhibitor of both smooth muscle cell proliferation and its synthesis of collagen (120), whereas ET-1 is a promoter of smooth muscle cell proliferation and the synthesis of collagen (121). It becomes apparent that local changes in wall shear stress from baseline conditions play important

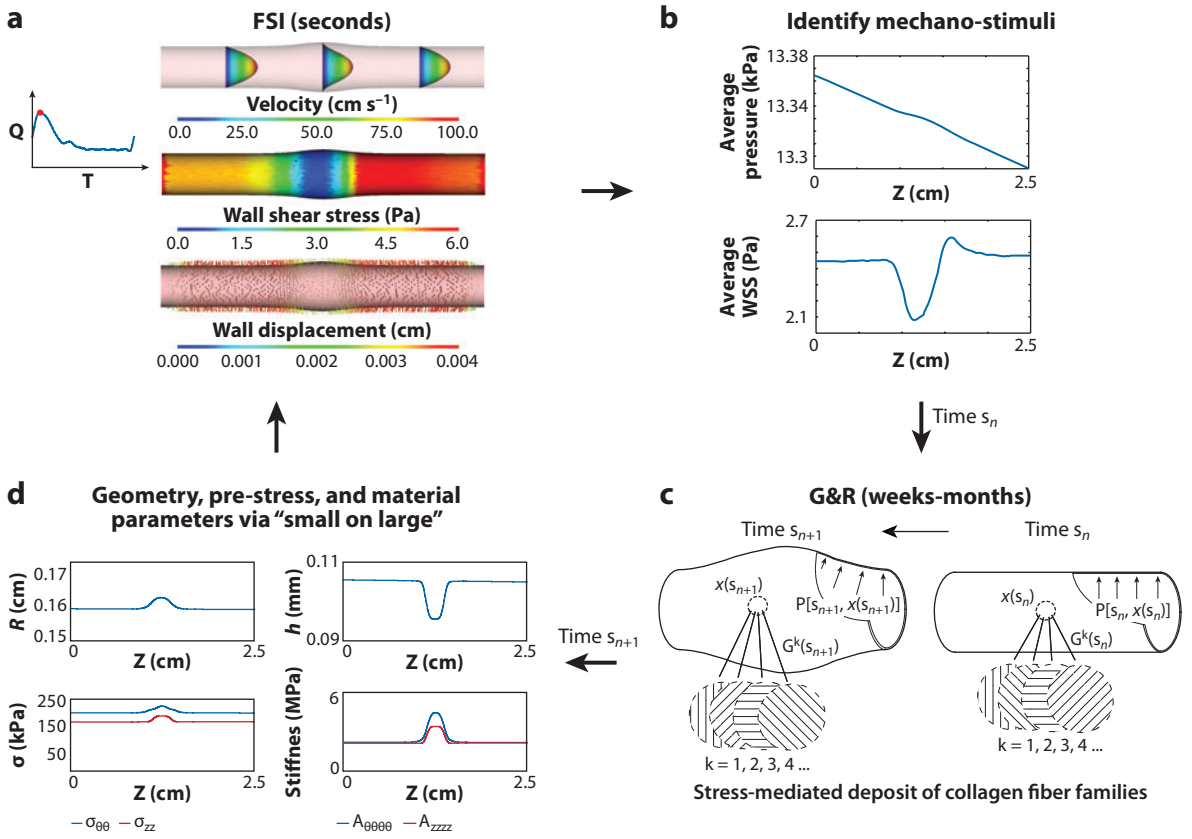


**Figure 8**

Iterative loop and information transferred in the coupling between the fluid-structure interactions (FSI) and growth and remodeling (G&R) parts of a fluid-solid-growth (FSG) framework. (*a*) FSI computation describing the hemodynamic state of the artery over the short timescale (seconds). (*b*) Identification of the biomechanical stimuli (in this case, tensile stress and wall shear stress) that elicit a G&R response. (*c*) G&R computation describing the evolution of vessel wall geometry, composition, and material properties over the long timescale (weeks to months). (*d*) Definition of a new linearized geometry, pre-stress, and material properties for the FSI computation.

roles in controlling smooth muscle cell contractility, and they also contribute to the rate and extent of cell and matrix turnover within the wall.

To understand hemodynamic-induced changes in vascular geometry, structure, and function, we must quantify the complexities of the flow field and the distribution of stress on and within the arterial wall on a patient-specific basis. Motivated by these and similar observations, Humphrey, Taylor, and colleagues (122) have brought together, for the first time, a fluid-solid growth (FSG) computational framework for solving the full 3D hemodynamics problem in patient-specific geometries and for solving the wall mechanics G&R problem, involving geometrically and materially nonlinear behaviors. The components of this multi-scale FSG framework are depicted in **Figure 8**. In this framework, the hemodynamic forces acting during the cardiac cycle provide the loads for the vascular G&R formulation, defined on a timescale of weeks to months, which in turn provides the updated geometry and material properties for the hemodynamic simulation. This framework is general enough to enable new data on stress-mediated growth and remodeling processes to be incorporated mathematically as they become available. For example, there

is a pressing need for data on which to build more comprehensive constitutive models for mass production and removal as a function of the evolving state of stress (or strain). Once validated in well-designed experiments, FSG modeling may become an essential tool in the understanding of diverse vascular pathologies, new clinical interventions (e.g., surgical planning), and the design of implantable medical devices.

## Optimal Treatment Plans

Numerical optimization methods combined with simulations of blood flow and vessel dynamics represent an important direction for patient-specific modeling. Marsden et al. described a shape optimization method for cardiovascular modeling based on a derivative-free approach using surrogates for increased efficiency together with mesh-adaptive direct search to guarantee convergence to a local minimum (123). As noted by Marsden et al., the main challenges relate to employing physiologically accurate and validated methods, assessing appropriate measures of performance (cost functions), implementing an optimization method appropriate for expensive, time-dependent, 3D fluid mechanics problems, and developing tools for the efficient parameterization of patient-specific geometries. Ultimately, optimization methods coupled with fluid-solid-growth methods could ensure that individual patients get the best possible hemodynamic outcomes in the near term and in the long term.

## Device Design and Evaluation

Advances in biomaterials have enabled the development of various medical devices to treat cardiovascular disease. Computational mechanics principles have been used for the design and evaluation of many of these devices, such as stents, stent-grafts, mechanical heart valves, blood pumps, and ventricular-assist devices.

Stents (bare metal or drug-eluting) are structures used to alleviate diminished blood flow to organs beyond an obstruction or stenosis to maintain an adequate delivery of oxygenated blood. The placement of these mechanical structures changes the biomechanical environment of the artery. Migliavacca and colleagues have investigated different geometric and mechanical factors involved in stent deployment (124, 125), Holzapfel and colleagues have studied the interactions of vascular stents with human atherosclerotic lesions (126), and LaDisa and colleagues have correlated stent design with alterations of wall shear stress and intima hyperplasia (127). Steiman (128) and Cebral (129) have investigated the altered hemodynamic conditions of flow in stented cerebral aneurysms.

Stent-grafts are stents covered with fabric that are primarily used to treat aortic aneurysms. These devices are usually delivered endovascularly. Stent-graft migration and endoleaks are the main complications associated with these devices. Morris and colleagues have performed a combined analytical and computational fluid dynamics (CFD) study of the forces acting on abdominal aortic aneurysm (AAA) stent-grafts (130). Li & Kleinstreuer (131) have simulated the fluid-structure interactions in a stented AAA model.

Mechanical heart pumps and ventricular-assist devices provide patients with cardiac failure with supplemental circulatory support until a transplant becomes available (132). There has been a shift in the use of these devices from a bridge therapy toward a destination therapy as a result of continuous improvements in device design and a lack of donors. The design of these devices presents important challenges in computational biomechanics, such as models for blood damage and thrombosis, device optimization for hydrodynamic efficiency and durability (133). Some of these issues are also shared by the design of mechanical heart valves (134).

In all instances presented here, it is paramount to have an understanding of the biomechanical environment experienced by the device in vivo to ensure its correct function and durability. However, the variability of this biomechanical environment from subject to subject is so large that the choice of device for the treatment of a particular patient should be made in a personalized manner.

## Verification and Validation

In order for computational methods to be accepted into clinical practice for planning cardiovascular surgery, extensive verification and validation is needed. Verification of a numerical method is defined as the assessment of the numerical accuracy with which the method is implemented in a computer. This process usually relies on the existence of an analytical solution for the method; however, the validation of a computational method is a more complex process because it involves comparing the results of the method with those observed in the real world (135). It is clear that, when developing new methods for cardiovascular modeling, the verification should precede any attempt of validation. A succinct and clear distinction between verification and validation is given by Roache (136), who describes verification as "solving the equations right," whereas validation is "solving the right equations."

Womersley's solution for pulsatile flow in a straight semi-infinite circular deformable vessel (137) represents an excellent framework to understand some of the principles that govern wave propagation and fluid-structure interaction phenomena in the cardiovascular system, and it is also a good tool to perform verification studies of mathematical models of blood flow in compliant arteries.

For more complex geometries, in vitro experimental data has been used to validate numerical methods (3). Ku and colleagues (138) performed a validation study of CFD data with MRI data in an in vitro bypass-graft model. Hoi et al. (139) developed a validation study of CFD methods with particle-image velocimetry (PIV) data in an in vitro model of a cerebral aneurysm.

Validation of numerical methods is considerably more challenging in vivo, where experiments are difficult to control and measurement data is challenging to acquire. Ku et al. compared calculated flow rates with measured flow rates obtained using MRI techniques in thoraco-thoraco aortic bypass procedures in eight pigs (140). The predicted and measured waveforms had similar shapes and amplitudes, and predicted flow distribution was within approximately 10% of the experimental data. More recently, Saloner and colleagues performed a comparison of CFD results and in vivo MRI measurements of flow in cerebral aneurysms (141). Although it appears that computational methods may be used effectively to predict flow distribution, experimental validation studies are preliminary. In addition, it is likely that prediction of in vivo flow-velocity profiles and pressure fields will present considerable challenges.

## DISCLOSURE STATEMENT

C.A. Taylor is a founder of Cardiovascular Simulation, Inc.

## ACKNOWLEDGMENTS

This review was supported, in part, by grants from the National Science Foundation (ITR-0205741) and the National Institutes of Health (U54 GM072970). We also acknowledge expert contributions to our research by E.J. Bekkers, C.P. Cheng, M.T. Draney, H.J. Kim, J.A. LaDisa, A.S. Les, A. Marsden, R.L. Spilker, I.E. Vignon-Clementel, K.C. Wang, and N.M. Wilson.

## LITERATURE CITED


1. Moore JA, Rutt BK, Karlik SJ, Yin K, Ethier CR. 1999. Computational blood flow modeling based on in vivo measurements. *Ann. Biomed. Eng.* 27:627–40
2. Taylor CA, Draney MT, Ku JP, Parker D, Steele BN, et al. 1999. Predictive medicine: computational techniques in therapeutic decision-making. *Comput. Aided Surg.* 4:231–47
3. Taylor CA, Hughes TJR, Zarins CK. 1998. Finite element modeling of blood flow in arteries. *Comput. Methods Appl. Mech. Eng.* 158:155–96
4. Long Q, Xu XY, Ariff B, Thom SA, Hughes AD, Stanton AV. 2000. Reconstruction of blood flow patterns in a human carotid bifurcation: a combined CFD and MRI study. *J. Magn. Reson. Imaging.* 11:299–311
5. Steinman DA. 2002. Image-based computational fluid dynamics modeling in realistic arterial geometries. *Ann. Biomed. Eng.* 30:483–97
6. Gijsen FJ, Wentzel JJ, Thury A, Lamers B, Schuurbiers JC, et al. 2007. A new imaging technique to study 3-D plaque and shear stress distribution in human coronary artery bifurcations in vivo. *J. Biomech.* 40:2349–57
7. Tang BT, Cheng CP, Draney MT, Wilson NM, Tsao PS, et al. 2006. Abdominal aortic hemodynamics in young healthy adults at rest and during lower limb exercise: quantification using image-based computer modeling. *Am. J. Physiol. Heart Circ. Physiol.* 291:H668–76
8. Cebral JR, Castro MA, Burgess JE, Pergolizzi RS, Sheridan MJ, Putman CM. 2005. Characterization of cerebral aneurysms for assessing risk of rupture by using patient-specific computational hemodynamics models. *Am. J. Neuroradiol.* 26:2550–9
9. Jou LD, Wong G, Dispensa B, Lawton MT, Higashida RT, et al. 2005. Correlation between lumenal geometry changes and hemodynamics in fusiform intracranial aneurysms. *Am. J. Neuroradiol.* 26:2357–63
10. Shojima M, Oshima M, Takagi K, Torii R, Hayakawa M, et al. 2004. Magnitude and role of wall shear stress on cerebral aneurysm: computational fluid dynamic study of 20 middle cerebral artery aneurysms. *Stroke* 35:2500–5
11. Vorp DA. 2007. Biomechanics of abdominal aortic aneurysm. *J. Biomech.* 40:1887–902
12. Bronskill MJ, Sprawls P, eds. 1992. *The Physics of MRI*. College Park, MD: AAPM Summer School. 527 pp.
13. Draney MT, Alley MT, Tang BT, Wilson NM, Herfkens RJ, Taylor CA. 2002. *Importance of 3d nonlinear gradient corrections for quantitative analysis of 3d MR angiographic data*. Presented at Int. Soc. Magn. Reson. Med. Mtg., 10th, Honolulu, HI
14. Kachelriess M, Ulzheimer S, Kalender WA. 2000. ECG-correlated imaging of the heart with subsecond multislice spiral CT. *IEEE Trans. Med. Imaging* 19:888–901
15. Pelc NJ, Bernstein MA, Shimakawa A, Glover GH. 1991. Encoding strategies for three-direction phase-contrast MR imaging of flow. *J. Magn. Reson. Imaging* 1:405–13
16. Pelc NJ, Herfkens RJ, Shimakawa A, Enzmann DR. 1991. Phase contrast cine magnetic resonance imaging. *Magn. Reson. Q.* 7:229–54
17. Pelc NJ, Sommer FG, Li KCP, Brosnan TJ, Herfkens RJ, Enzmann DR. 1994. Quantitative magnetic resonance flow imaging. *Magn. Reson. Q.* 10:125–47
18. Russ JC. 1999. *The Image Processing Handbook*. Boca Raton, FL: CRC
19. Kass M, Witkin A, Terzopoulos D. 1987. Snakes: active contour models. *Int. J. Comput. Vis.* 1:321–31
20. McInerney T, Terzopoulos D. 1995. A dynamic finite element surface model for segmentation and tracking in multidimensional medical images with application to cardiac 4D image analysis. *Comput. Med. Imaging Graph.* 19:69–83
21. McInerney T, Terzopoulos D. 1996. Deformable models in medical image analysis: a survey. *Med. Image Anal.* 1(2):91–108
22. Cohen L, Cohen I. 1993. Finite element methods for active contour models and balloons for 2D and 3D images. *IEEE Trans. Pattern Anal. Mach. Intell.* 15(11):1131–47
23. Malladi R, Kimmel R, Adalsteinsson D, Sapiro G, Caselles V, Sethian JA. 1996. A geometric approach to segmentation and analysis of 3D medical images. *Proc. IEEE Workshop Math. Methods Biomed. Image Anal.*, San Francisco, CA

24. Caselles V, Catte F, Coll T, Dibos F. 1993. A geometric model for active contours in image processing. *Numeri. Math.* 66:1–31
25. Sethian JA. 1999. *Level Set Methods and Fast Marching Methods*. Cambridge, England: Cambridge Univ. Press
26. Caselles V, Kimmel R, Sapiro G. 1997. Geodesic active contours. *Int. J. Comput. Vis.* 22:61–79
27. Kichenassamy A, Kumar A, Olver P, Tannenbaum A, Yezzi A. 1995. *Gradient flows and geometric active contour models*. Presented at Int. Conf. Comput. Vis., 5th, Boston, MA
28. Wang KC, Dutton RW, Taylor CA. 1999. Improving geometric model construction for blood flow modeling. *IEEE Eng. Med. Biol. Mag.* 18:33–39
29. Antiga L, Piccinelli M, Botti L, Ene-Iordache B, Remuzzi A, Steinman DA. 2008. An image-based modeling framework for patient-specific computational hemodynamics. *Med. Biol. Eng. Comput.* 46:1097–112
30. Cebral JR, Castro MA, Appanaboyina S, Putman CM, Millan D, Frangi AF. 2005. Efficient pipeline for image-based patient-specific analysis of cerebral aneurysm hemodynamics: technique and sensitivity. *IEEE Trans. Med. Imaging* 24:457–67
31. Rayz VL, Boussel L, Lawton MT, Acevedo-Bolton G, Ge L, et al. 2008. Numerical modeling of the flow in intracranial aneurysms: prediction of regions prone to thrombus formation. *Ann. Biomed. Eng.* 36:1793–804
32. Torii R, Oshima M, Kobayashi T, Takagi K, Tezduyar TE. 2008. Fluid-structure interaction modeling of a patient-specific cerebral aneurysm: influence of structural modeling. *Comput. Mech.* 43:151–59
33. Bekkers EJ, Taylor CA. 2008. Multiscale vascular surface model generation from medical imaging data using hierarchical features. *IEEE Trans. Med. Imaging* 27:331–41
34. Prakash S, Ethier CR. 2001. Requirements for mesh resolution in 3D computational hemodynamics. *J. Biomech. Eng.* 123:134–44
35. Peattie RA, Riehle TJ, Bluth EI. 2004. Pulsatile flow in fusiform models of abdominal aortic aneurysms: flow fields, velocity patterns and flow-induced wall stresses. *J. Biomech. Eng.* 126:438–46
36. Salsac AV, Sparks SR, Lasheras JC. 2004. Hemodynamic changes occurring during the progressive enlargement of abdominal aortic aneurysms. *Ann. Vasc. Surg.* 18:14–21
37. Müller J, Sahni O, Li X, Jansen KE, Shephard MS, Taylor CA. 2005. Anisotropic adaptive finite element method for modelling blood flow. *Comput. Methods Biomech. Biomed. Eng.* 8:295–305
38. Sahni O, Müller J, Jansen KE, Shephard MS, Taylor CA. 2006. Efficient anisotropic adaptive discretization of the cardiovascular system. *Comput. Methods Appl. Mech. Eng.* 195:5634–55
39. Sahni O, Jansen KE, Shephard MS, Taylor CA, Beall MW. 2008. Adaptive boundary layer meshing for viscous flow simulations. *Eng. Comput.* 24:267–85
40. Perktold K, Resch M, Peter RO. 1991. Three-dimensional numerical analysis of pulsatile flow and wall shear stress in the carotid artery bifurcation. *J. Biomech.* 24:409–20
41. Taylor CA, Hughes TJ, Zarins CK. 1998. Finite element modeling of three-dimensional pulsatile flow in the abdominal aorta: relevance to atherosclerosis. *Ann. Biomed. Eng.* 26:975–87
42. Lagana K, Balossino R, Migliavacca F, Pennati G, Bove EL, et al. 2005. Multiscale modeling of the cardiovascular system: application to the study of pulmonary and coronary perfusions in the univentricular circulation. *J. Biomech.* 38:1129–41
43. Migliavacca F, Balossino R, Pennati G, Dubini G, Hsia TY, et al. 2006. Multiscale modelling in biofluidynamics: application to reconstructive pediatric cardiac surgery. *J. Biomech.* 39:1010–20
44. Vignon-Clementel IE, Figueroa CA, Jansen KC, Taylor CA. 2006. Outflow boundary conditions for three-dimensional finite element modeling of blood flow and pressure in arteries. *Comput. Methods Appl. Mech. Eng.* 195:3776–96
45. Formaggia L, Gerbeau JF, Nobile F, Quarteroni A. 2001. On the coupling of 3D and 1D Navier-Stokes equations for flow problems in compliant vessels. *Comput. Methods Appl. Mech. Eng.* 191:561–82
46. Vignon I, Taylor CA. 2004. Outflow boundary conditions for one-dimensional finite element modeling of blood flow and pressure waves in arteries. *Wave Motion* 39:361–74
47. Spilker RL, Feinstein JA, Parker DW, Reddy VM, Taylor CA. 2007. Morphometry-based impedance boundary conditions for patient-specific modeling of blood flow in pulmonary arteries. *Ann. Biomed. Eng.* 35:546–59

48. Spilker RL, Vignon-Clementel IE, Figueroa CA, Taylor CA. 2007. *A Systematic Method for Tuning Three-dimensional Patient-specific Hemodynamic Simulations with 3-element Windkessel Outlet Boundary Conditions*. Presented at U.S. Nat. Congr. Comput. Mech., 9th, San Francisco, CA
49. Figueroa CA, Vignon-Clementel IE, Jansen KC, Hughes TJR, Taylor CA. 2006. A coupled momentum method for modeling blood flow in three-dimensional deformable arteries. *Comput. Methods Appl. Mech. Eng.* 195:5685–706
50. Formaggia L, Moura A, Nobile F. 2007. On the stability of the coupling of 3D and 1D fluid-structure interaction models for blood flow simulations. *ESAIM: Math. Model. Numer. Anal.* 41:743–69
51. Kim HJ, Figueroa CA, Hughes TJR, Jansen KE, Taylor CA. 2009. Augmented lagrangian method for constraining the shape of velocity profiles at outlet boundaries for three-dimensional finite element simulations of blood flow. *Comput. Methods Appl. Mech. Eng.* In press
52. Hughes TJR, Liu WK, Zimmermann TK. 1981. Lagrangian–Eulerian finite element formulation for incompressible viscous flows. *Comput. Methods Appl. Mech. Eng.* 29:329–49
53. Le Tallec P, Mouro J. 2001. Fluid structure interaction with large structural displacements. *Comput. Methods Appl. Mech. Eng.* 190:3039–67
54. Perktold K, Rappitsch G. 1995. Computer simulation of local blood flow and vessel mechanics in a compliant carotid artery bifurcation model. *J. Biomech.* 28:845–56
55. Prosi M, Perktold K, Ding Z, Friedman MH. 2004. Influence of curvature dynamics on pulsatile coronary artery flow in a realistic bifurcation model. *J. Biomech.* 37:1767–75
56. Gerbeau J-F, Vidrascu M, Frey P. 2005. Fluid-structure interaction in blood flows on geometries based on medical imaging. *Comput. Struct.* 83:155–65
57. Gerbeau J-F, Vidrascu M. 2003. A quasi-Newton algorithm based on a reduced model for fluid-structure interaction problems in blood flows. *Math. Model. Numer. Anal.* 37:631–47
58. Fernandez MA, Gerbeau J-F, Grandmont C. 2007. A projection semi-implicit scheme for the coupling of an elastic structure with an incompressible fluid. *Int. J. Numer. Methods Eng.* 69:794–821
59. Bazilevs Y, Calo VM, Zhang Y, Hughes TJR. 2006. Isogeometric fluid-structure interaction analysis with applications to arterial blood flow. *Comput. Mech.* 38:310–22
60. Zhang Y, Bazilevs Y, Goswami S, Bajaj CL, Hughes TJR. 2007. Patient-specific vascular NURBS modeling for isogeometric analysis of blood flow. *Comput. Methods Appl. Mech. Eng.* 196:2943–59
61. Wolters B, Rutten MCM, Schurink GWH, Kose U, de Hart J, van de Vosse FN. 2005. A patient-specific computational model of fluid-structure interaction in abdominal aortic aneurysms. *Med. Eng. Phys.* 27:871–83
62. Peskin CS. 1972. Flow patterns around heart valves: a numerical method. *J. Comput. Phys.* 10:252–71
63. Peskin CS. 2003. The immersed boundary method. *Acta Numer.* 11:479–517
64. Lemmon JD, Yoganathan AP. 2000. Computational modeling of left heart diastolic function: Examination of ventricular dysfunction. *J. Biomech. Eng.* 122:297–303
65. Watton PN, Luo XY, Wang X, Bernacca GM, Molloy P, Wheatley DJ. 2007. Dynamic modelling of prosthetic chorded mitral valves using the immersed boundary method. *J. Biomech.* 40:613–23
66. Vigmond EJ, Clements C, McQueen DM, Peskin CS. 2008. Effect of bundle branch block on cardiac output: a whole heart simulation study. *Prog. Biophys. Mol. Biol.* 97:520–42
67. Bagchi P. 2007. Mesoscale simulation of blood flow in small vessels. *Biophys. J.* 92:1858–77
68. Glowinski R, Pan TW, Periaux J. 1997. A Lagrange multiplier/fictitious domain method for the numerical simulation of incompressible viscous flow around moving rigid bodies: (I) case where the rigid body motions are known a priori. *C. R. Acad. Sci. Ser. I Math.* 324:361–69
69. Baaijens FPT. 2001. A fictitious domain/mortar element method for fluid-structure interaction. *Int. J. Numer. Methods Fluids* 35:743–61
70. De Hart J, Peters GWM, Schreurs PJG, Baaijens FPT. 2003. A three-dimensional computational analysis of fluid-structure interaction in the aortic valve. *J. Biomech.* 36:103–12
71. De Hart J, Peters GWM, Schreurs PJG, Baaijens FPT. 2004. Collagen fibers reduce stresses and stabilize motion of aortic valve leaflets during systole. *J. Biomech.* 37:303–11
72. van de Vosse FN, de Hart J, van Oijen C, Bessems D, Gunther TWM, et al. 2003. Finite-element-based computational methods for cardiovascular fluid-structure interaction. *J. Eng. Math.* 47:335–68

73. van Loon R, Anderson PD, van de Vosse FN. 2006. A fluid-structure interaction method with solid-rigid contact for heart valve dynamics. *J. Comput. Phys.* 217:806–23
74. Tezduyar TE, Behr M, Liou J. 1992. A new strategy for finite-element computations involving moving boundaries and interfaces—the deforming-spatial-domain space-time procedure: I. the concept and the preliminary numerical tests. *Comput. Methods Appl. Mech. Eng.* 94:339–51
75. Kim HJ, Figueroa CA, Vignon-Clementel IE, Jansen KE, Taylor CA. 2007. *Three-dimensional simulations of aortic blood flow and pressure including a lumped heart model*. Presented at U.S. Nat. Congr. Comput. Mech., 9th, San Francisco, CA
76. Caro CG, Fitz-Gerald JM, Schroter RC. 1971. Atheroma and arterial wall shear. Observation, correlation and proposal of a shear dependent mass transfer mechanism for atherogenesis. *Proc. R. Soc. Lond. B Biol. Sci.* 177:109–59
77. Friedman MH, Hutchins GM, Bargeron CB, Deters OJ, Mark FF. 1981. Correlation between intimal thickness and fluid shear in human arteries. *Atherosclerosis* 39:425–36
78. Zarins CK, Giddens DP, Bharadvaj BK, Sottiurai VS, Mabon RF, Glagov S. 1983. Carotid bifurcation atherosclerosis. Quantitative correlation of plaque localization with flow velocity profiles and wall shear stress. *Circ. Res.* 53:502–14
79. Glagov S, Weisenberg E, Zarins CK, Stankunavicius R, Kolettis GJ. 1987. Compensatory enlargement of human atherosclerotic coronary arteries. *N. Engl. J. Med.* 316:1371–75
80. Moore JA, Steinman DA, Ethier CR. 1998. Computational blood flow modeling: errors associated with reconstructing finite element models from magnetic resonance images. *J. Biomech.* 31:179–84
81. Moore JA, Steinman DA, Holdsworth DW, Ethier CR. 1999. Accuracy of computational hemodynamics in complex arterial geometries reconstructed from magnetic resonance imaging. *Ann. Biomed. Eng.* 27:32–41
82. Antiga L, Steinman DA. 2004. Robust and objective decomposition and mapping of bifurcating vessels. *IEEE Trans. Med. Imaging* 23:704–13
83. Thomas JB, Antiga L, Che SL, Milner JS, Steinman DA, et al. 2005. Variation in the carotid bifurcation geometry of young versus older adults: implications for geometric risk of atherosclerosis. *Stroke* 36:2450–56
84. Xu XY, Long Q, Collins MW, Bourne M, Griffith TM. 1999. Reconstruction of blood flow patterns in human arteries. *Proc. Inst. Mech. Eng. H* 213:411–21
85. Long Q, Ariff B, Zhao SZ, Thom SA, Hughes AD, Xu XY. 2003. Reproducibility study of 3D geometrical reconstruction of the human carotid bifurcation from magnetic resonance images. *Magn. Reson. Med.* 49:665–74
86. Dai G, Kaazempur-Mofrad MR, Natarajan S, Zhang Y, Vaughn S, et al. 2004. Distinct endothelial phenotypes evoked by arterial waveforms derived from atherosclerosis-susceptible and -resistant regions of human vasculature. *Proc. Natl. Acad. Sci. USA* 101:14871–76
87. Moore J, Ku D. 1994. Pulsatile velocity measurements in a model of the human abdominal aorta under simulated exercise and postprandial conditions. *J. Biomech. Eng.* 116:107–11
88. Moore JE Jr, Ku DN, Zarins CK, Glagov S. 1992. Pulsatile flow visualization in the abdominal aorta under differing physiologic conditions: implications for increased susceptibility to atherosclerosis. *J. Biomech. Eng.* 114:391–97
89. Moore JE Jr, Maier SE, Ku DN, Boesiger P. 1994. Hemodynamics in the abdominal aorta: a comparison of in vitro and in vivo measurements. *J. Appl. Physiol.* 76:1520–27
90. Moore JE Jr, Xu C, Glagov S, Zarins CK, Ku DN. 1994. Fluid wall shear stress measurements in a model of the human abdominal aorta: oscillatory behavior and relationship to atherosclerosis. *Atherosclerosis* 110:225–40
91. Taylor CA, Hughes TJ, Zarins CK. 1999. Effect of exercise on hemodynamic conditions in the abdominal aorta. *J. Vasc. Surg.* 29:1077–89
92. Greve JM, Les AS, Tang BT, Draney Blomme MT, Wilson NM, et al. 2006. Allometric scaling of wall shear stress from mice to humans: quantification using cine phase-contrast MRI and computational fluid dynamics. *Am. J. Physiol. Heart Circ. Physiol.* 291:H1700–8

93. Feintuch A, Ruengsakulrach P, Lin A, Zhang J, Zhou YQ, et al. 2007. Hemodynamics in the mouse aortic arch as assessed by MRI, ultrasound, and numerical modeling. *Am. J. Physiol. Heart Circ. Physiol.* 292:H884–92
94. Suo J, Ferrara DE, Sorescu D, Guldberg RE, Taylor WR, Giddens DP. 2007. Hemodynamic shear stresses in mouse aortas: implications for atherogenesis. *Arterioscler. Thromb. Vasc. Biol.* 27:346–51
95. Humphrey JD, Taylor CA. 2008. Intracranial and abdominal aortic aneurysms: similarities, differences, and need for a new class of computational models. *Annu. Rev. Biomed. Eng.* 10:221–46
96. Acevedo-Bolton G, Jou LD, Dispensa BP, Lawton MT, Higashida RT, et al. 2006. Estimating the hemodynamic impact of interventional treatments of aneurysms: numerical simulation with experimental validation: technical case report. *Neurosurgery* 59:E429–30; author reply E-30
97. Castro MA, Putman CM, Cebral JR. 2006. Patient-specific computational modeling of cerebral aneurysms with multiple avenues of flow from 3D rotational angiography images. *Acad. Radiol.* 13:811–21
98. Castro MA, Putman CM, Cebral JR. 2006. Patient-specific computational fluid dynamics modeling of anterior communicating artery aneurysms: a study of the sensitivity of intra-aneurysmal flow patterns to flow conditions in the carotid arteries. *Am. J. Neuroradiol.* 27:2061–68
99. Cebral JR, Pergolizzi RS Jr, Putman CM. 2007. Computational fluid dynamics modeling of intracranial aneurysms: qualitative comparison with cerebral angiography. *Acad. Radiol.* 14:804–13
100. Oshima M, Kobayashi T, Takagi K. 2002. Biosimulation and visualization: effect of cerebrovascular geometry on hemodynamics. *Ann. N. Y. Acad. Sci.* 972:337–44
101. Shojima M, Oshima M, Takagi K, Torii R, Nagata K, et al. 2005. Role of the bloodstream impacting force and the local pressure elevation in the rupture of cerebral aneurysms. *Stroke* 36:1933–38
102. Boussel L, Rayz V, McCulloch C, Martin A, Acevedo-Bolton G, et al. 2008. Aneurysm growth occurs at region of low wall shear stress: patient-specific correlation of hemodynamics and growth in a longitudinal study. *Stroke* 39:2997–3002
103. Wilson NM, Arko FR, Taylor CA. 2005. Predicting changes in blood flow in patient-specific operative plans for treating aortoiliac occlusive disease. *Comput. Aided Surg.* 10:257–77
104. Wilson NM, Wang KC, Dutton RW, Taylor CA. 2001. A software framework for creating patient specific geometric models from medical imaging data for simulation based medical planning of vascular surgery. *Lect. Notes Comput. Sci.* 2208:449–56
105. Pekkan K, Kitajima HD, de Zelicourt D, Forbess JM, Parks WJ, et al. 2005. Total cavopulmonary connection flow with functional left pulmonary artery stenosis: angioplasty and fenestration in vitro. *Circulation* 112:3264–71
106. Whitehead KK, Pekkan K, Kitajima HD, Paridon SM, Yoganathan AP, Fogel MA. 2007. Nonlinear power loss during exercise in single-ventricle patients after the Fontan: insights from computational fluid dynamics. *Circulation* 116:I165–71
107. Bove EL, de Leval MR, Migliavacca F, Balossino R, Dubini G. 2007. Toward optimal hemodynamics: computer modeling of the Fontan circuit. *Pediatr. Cardiol.* 28(6):477–81
108. Dubini G, Migliavacca F, Pennati G, de Leval MR, Bove EL. 2004. Ten years of modelling to achieve haemodynamic optimisation of the total cavopulmonary connection. *Cardiol. Young* 14(Suppl. 3):48–52
109. Migliavacca F, Dubini G, Bove EL, de Leval MR. 2003. Computational fluid dynamics simulations in realistic 3-D geometries of the total cavopulmonary anastomosis: the influence of the inferior caval anastomosis. *J. Biomech. Eng.* 125:805–13
110. Marsden AL, Bernstein A, Reddy VM, Shadden S, Spilker RL, et al. 2008. Evaluation of a Novel Y-Shaped Extracardiac Fontan Baffle Using Computational Fluid Dynamics. *J. Thorac. Cardiovasc. Surg.* 137:394–403
111. Woodrum DA, Romano AJ, Lerman A, Pandya UH, Brosh D, et al. 2006. Vascular wall elasticity measurement by magnetic resonance imaging. *Magn. Reson. Med.* 56:593–600
112. Sermesant M, Moireau P, Camara O, Sainte-Marie J, Andriantsimiavona R, et al. 2006. Cardiac function estimation from MRI using a heart model and data assimilation: advances and difficulties. *Med. Image Anal.* 10:642–56
113. Humphrey JD. 2008. Vascular adaptation and mechanical homeostasis at tissue, cellular, and subcellular levels. *Cell Biochem. Biophys.* 50:53–78

114. Taber LA. 1998. A model for aortic growth based on fluid shear and fiber stresses. *J. Biomech. Eng.* 120:348–54
115. Rachev A. 2000. A model of arterial adaptation to alterations in blood flow. *J. Elast.* 61:83–111
116. Humphrey JD, Rajagopal KR. 2002. A constrained mixture model for growth and remodeling of soft tissues. *Math. Model. Methods Appl. Sci.* 12:407–30
117. Watton PN, Hill NA, Heil M. 2004. A mathematical model for the growth of the abdominal aortic aneurysm. *Biomech. Model. Mechanobiol.* 3:98–113
118. Kuhl E, Holzapfel GA. 2007. A continuum model for remodeling in living structures. *J. Mater. Sci.* 42:8811–23
119. Newby AC. 2006. Matrix metalloproteinases regulate migration, proliferation, and death of vascular smooth muscle cells by degrading matrix and nonmatrix substrates. *Cardiovasc. Res.* 69:614–24
120. Rizvi MAD, Myers PR. 1997. Nitric oxide modulates basal and endothelin-induced coronary artery vascular smooth muscle cell proliferation and collagen levels. *J. Mol. Cell. Cardiol.* 29:1779–89
121. Rizvi MAD, Katwa L, Spadone DP, Myers PR. 1996. The effects of endothelin-1 on collagen type I and type III synthesis in cultured porcine coronary artery vascular smooth muscle cells. *J. Mol. Cell. Cardiol.* 28:243–52
122. Figueroa CA, Baek S, Taylor CA, Humphrey JD. 2009. A computational framework for fluid-solid-growth modeling in cardiovascular simulations. *Comput. Methods Appl. Mech. Eng.* In press
123. Marsden AL, Feinstein JA, Taylor CA. 2008. A computational framework for derivative-free optimization of cardiovascular geometries. *Comput. Methods Appl. Mech. Eng.* 197:1890–905
124. Migliavacca F, Petrini L, Colombo M, Auricchio F, Pietrabissa R. 2002. Mechanical behavior of coronary stents investigated through the finite element method. *J. Biomech.* 35:803–11
125. Migliavacca F, Gervasco F, Prosi M, Zunino P, Minisini S, et al. 2007. Expansion and drug elution model of a coronary stent. *Comput. Methods Biomech. Biomed. Eng.* 10:63–73
126. Kiousis DE, Gasser TC, Holzapfel GA. 2007. A numerical model to study the interaction of vascular stents with human atherosclerotic lesions. *Ann. Biomed. Eng.* 35:1857–69
127. LaDisa JF, Olson LE, Molthen RC, Hettrick DA, Pratt PF, et al. 2005. Alterations in wall shear stress predict sites of neointimal hyperplasia after stent implantation in rabbit iliac arteries. *Am. J. Physiol. Heart Circ. Physiol.* 288:H2465–75
128. Stuhne GR, Steinman DA. 2004. Finite-element modeling of the hemodynamics of stented aneurysms. *J. Biomech. Eng.* 126:382–87
129. Cebral JR, Lohner R. 2005. Efficient simulation of blood flow past complex endovascular devices using an adaptive embedding technique. *IEEE Trans. Med. Imaging* 24:468–76
130. Morris L, Delassus P, Walsh M, McGloughlin T. 2004. A mathematical model to predict the in vivo pulsatile drag forces acting on bifurcated stent grafts used in endovascular treatment of abdominal aortic aneurysms (AAA). *J. Biomech.* 37:1087–95
131. Li ZH, Kleinstreuer C. 2005. Blood flow and structure interactions in a stented abdominal aortic aneurysm model. *Med. Eng. Phys.* 27:369–82
132. Simon MA, Watson J, Baldwin JT, Wagner WR, Borovetz HS. 2008. Current and future considerations in the use of mechanical circulatory support devices. *Annu. Rev. Biomed. Eng.* 10:59–84
133. Arora D, Behr M, Pasquali M. 2006. Hemolysis estimation in a centrifugal blood pump using a tensor-based measure. *Artif. Organs* 30:539–47
134. Alemu Y, Bluestein D. 2007. Flow-induced platelet activation and damage accumulation in a mechanical heart valve: numerical studies. *Artif. Organs* 31:677–88
135. Babuska I, Oden JT. 2004. Verification and validation in computational engineering and science: basic concepts. *Comput. Methods Appl. Mech. Eng.* 193:4057
136. Roache PJ. 1998. *Verification and Validation in Computational Science and Engineering*. Albuquerque, NM: Hermosa Publishers
137. Womersley JR. 1955. Oscillatory motion of a viscous liquid in a thin-walled elastic tube. I: the linear approximation for long waves. *Philos. Mag.* 7:199–221
138. Ku JP, Elkins CJ, Taylor CA. 2005. Comparison of CFD and MRI flow and velocities in an in vitro large artery bypass graft model. *Ann. Biomed. Eng.* 33:257–69

139. Hoi Y, Woodward SH, Kim M, Taulbee DB, Meng H. 2006. Validation of CFD simulations of cerebral aneurysms with implication of geometric variations. *J. Biomech. Eng. Trans. ASME* 128:844–51
140. Ku JP, Draney MT, Arko FR, Lee WA, Chan FP, et al. 2002. In vivo validation of numerical prediction of blood flow in arterial bypass grafts. *Ann. Biomed. Eng.* 30:743–52
141. Rayz VL, Boussel L, Acevedo-Bolton G, Martin AJ, Young WL, et al. 2008. Numerical simulations of flow in cerebral aneurysms: comparison of CFD results and in vivo MRI measurements. *J. Biomech. Eng. Trans. ASME* 130:051011